IPPI
Polyolefins Journal, Vol. 11, No. 3 (2024)
DOI: 10.22063/POJ.2024.3641.1311
ORIGINAL PAPER

Radiation shielding characteristics of HDPE/tungsten oxide nanocomposites reinforced with graphene oxide and LDPE using Geant4, XCOM and experiment

Shahryar Malekie[1,2*], Mohammad Amin Hosseini[3,4], Ahmadreza Abiz[5], Fatemeh Bolourinovin[1], Suffian Mohamad Tajudin[2]

[1]Radiation Application Research School, Nuclear Science and Technology Research Institute (NSTRI), P.O. Box 3148643111, Karaj, Iran
[2]School of Medical Imaging, Faculty of Health Sciences, Universiti Sultan Zainal Abidin (UniSZA), Terengganu, Malaysia
[3]Ionizing and Non-Ionizing Radiation Protection Research Center (INIRPRC), School of Paramedical Sciences, Shiraz University of Medical Sciences, Shiraz, Iran
[4]Physics Department, Università degli Studi di Torino, Turin, Italy
[5]Department of Nuclear Engineering, Islamic Azad University Arsanjan Branch, Arsanjan, Iran

Received: 26 May 2024, Accepted: 8 July 2024

ABSTRACT

This research aims to determine and quantify the radiation shielding characteristics of high-density polyethylene/tungsten oxide ($HDPE/WO_3$) nanocomposites including the linear attenuation coefficient (μ), mass attenuation coefficient (μ/ρ), half-value layer (HVL) and tenth-value layer (TVL) for photons at various energies using Geant4, XCOM, and experiment. Thus, HDPE was chosen as the polymer matrix. Then, the samples at various concentrations of WO_3 nanoparticles (0, 1, 2, 3, 4, 5, 6, and 9.5 wt.%), different graphene oxide (GO) weight percentages (0, 0.25, 0.5, and 1 wt.%), and 10 and 20 wt.% linear low-density polyethylene (LLDPE) were fabricated. An NaI (Tl) scintillation detector was used to measure the shielding quantities using the ^{201}Tl, and ^{99m}Tc sources at three energies of 135, 140, and 167 keV. The experimental results demonstrated that the addition of GO and LLDPE to the HDPE matrix resulted in a more uniform sample. Incorporating 20% LLDPE into the HDPE polymer matrix for the ^{99m}Tc resulted in an 18% rise in μ compared to pure HDPE. Finally, the experimental results revealed a comparatively good agreement with the Geant4 and XCOM simulations. **Polyolefins J (2024) 11: 199-211**

Keywords: Radiation shielding characteristics; WO_3/HDPE nanocomposite; Geant4 simulation; XCOM; solution processing.

INTRODUCTION

In the present era, a noticeable transition has occurred in the field of radiation shielding, with polymer composites emerging as viable substitutes for traditional materials such as lead (Pb). This shift is primarily motivated by the need to address the environmental and health concerns associated with conventional radiation shields. Lead-free materials, such as heavy metal oxide particles like tungsten oxide (WO_3), have been increasingly utilized in polymer matrices, making them innovative materials for attenuation of gamma and X-rays in diagnostic applications. This incorporation of alternative materials has gained popularity due to the desire to move away from traditional lead-based options [1-10]. Heavy metal oxide materials demonstrate superior high-effective atomic number properties, thereby improving radiation shielding effectiveness. Consequently, they are highly proficient in attenuating low-energy gamma and X-rays. There are several studies related to nanocomposites in radiation shielding and recent advancements in Monte Carlo simulations [11-19].

*Corresponding Author - E-mail: smaleki@aeoi.org.ir

CC BY NC SA

In this work, WO_3 nanoparticles were considered as the main constituent of the shielding material for gamma-rays at low energy level. The reasons for choosing WO_3 as the main filler in this polymer composite can be summarized as follows: Firstly, WO_3 nanoparticles have a density of 7.16 g/cm^3, which makes them suitable for radiation protection purposes and has shown good performance in previous studies [1, 20, 21]. Also, WO_3 nanoparticles are nano-fillers that possess a remarkable surface-to-volume ratio, making them highly efficient in radiation shielding applications. Compared to micro-fillers, these nano-fillers demonstrate a significantly higher photon absorption cross section when exposed to gamma or X-rays at low energies [1]. This enhanced capability to absorb radiation is attributed to their smaller size and increased surface area, allowing for more effective interaction with the incoming radiation.

Furthermore, the K-edge absorption threshold of tungsten, characterized by an atomic number of 74 and a density of 19.3 g/cm^3, is positioned at energy of 70 keV, thus making it well-suited for applications in the diagnostic range. It is worth mentioning that at lower energies and near the K-edge absorption edge, the dominant effect is photoelectric. Furthermore, compared to lead, WO_3 produces fewer secondary radiations and significantly mitigates the challenges associated with the toxicity of lead.

Following the presentation of heavy metal oxide tungsten oxide as the primary filler material in the composite coating, attention is now turned towards introducing the polymer matrix and its features in this study. Polyethylene is one of the most important and widely used types of polymers known in the world. It is classified into five categories based on density: low-density polyethylene (LDPE), linear low-density polyethylene (LLDPE), high-density polyethylene (HDPE), medium-density polyethylene (MDPE), and ultra-high molecular weight polyethylene (UHMWPE). Generally, HDPE has higher density and crystallinity compared to LDPE. In fact, the atomic structure of HDPE consists of two parts: amorphous and crystalline. The addition of WO_3 filler to HDPE is mainly possible in the amorphous region, while the crystalline part, due to strong molecular bonds, hinders the incorporation of the filler material [22]. However, since there is limited space for adding fillers in the polymer matrix, it is necessary to use fillers with small dimensions. That is why in current research, nanoscale fillers are used in the polymer matrix. Furthermore, it has been shown that materials such as graphene oxide (GO) and LLDPE can contribute to the formation of new bonds with the main matrix [23, 24]. As a result, it allows for an increase in the weight percentage of WO_3 and is expected to provide a more uniform dispersion.

The Monte Carlo method is considered to be an accurate computational technique for evaluating the protective characteristics of composite materials. It has proven to be effective in estimating the safety properties of such materials. This method is widely utilized due to its reliability and ability to provide precise results in the assessment of composite materials' protective features. Numerous research investigations have utilized the Monte Carlo technique to analyze the effectiveness of radiation shielding in micro/nano composites [25-31]. To assess these applications, the widely used MCNP code, which rely on the Monte Carlo method, is typically employed. Geant4 is a computational code based on the Monte Carlo method that is less frequently utilized compared to the widely used MCNP code.

In this work, radiation shielding characteristics including linear attenuation coefficient (μ), mass attenuation coefficient (μ/ρ), half-value layer (HVL) and tenth-value layer (TVL) of HDPE/WO_3 nanocomposites reinforced with GO, and LLDPE at various concentrations of the inclusions for photons at various energies were explored using Geant4, XCOM and experiment.

EXPERIMENTAL

Preparation the materials and instruments

In this experimental work, HDPE (grade 52518), and LLDPE (grade 209), respectively, with densities of 0.95, and 0.92 g/cm^3 were purchased from Iranian Petrochemical Company (Bandar Imam). The selection of LLDPE was based on its elevated melt flow index (MFI). A higher MFI in a polymer corresponds to a higher branching percentage [32]. Consequently, this higher branching percentage enables a greater incorporation of nanoparticles into the polymer matrix.

The WO_3 nanopowder, density of 7.16 g/cm^3, pale yellow in color and particle size 20-66 nm and GO nanopowder, density of 2.1 g/cm^3, dimensions less than 50 μm and thickness of 3.4-7nm were obtained from US-Nano company. Also, o-Xylene (ortho-xylene) solvent was utilized from Merck KGaA, Germany, due to its boiling point being closer to the

melting temperature of polyethylene.

Instruments and experimental setup

The experiments were performed at the Secondary Standard Dosimetry Laboratory (SSDL) of Karaj-Iran. In order to distribute the WO_3 nanoparticles homogeneously in the polymer matrix, an ultrasonic bath (model Elmasonic E60H, 500 W) was used. Subsequent to the fabrication process, an analysis of the dispersion states of the inclusions in the polymer matrix, along with an assessment of the constituents of the composite materials, was conducted through scanning electron microscopy (SEM, TESCAN Vega 3, at 20 kV) and energy-dispersive X-ray spectroscopy (EDS or EDAX) at the Razi Metallurgical Research Center in Iran.

To measure the radiation shielding properties of the samples against the gamma-rays of various radioactive sources namely Thallium-201 (^{201}Tl), and technetium-99m (^{99m}Tc), at three energies of 135, 140, and 167 keV, a NaI (Tl) detector (Model NT-800-Novin Teyf Company, Iran) was used to read the count both with and without the radiation shields (I_0 and I) at different thicknesses. The multichannel analyzer (MCA) operating voltage was adjusted to 750 V at time intervals of 60 s. Each measurement was repeated four times.

The details of the applied sources exhibiting the gamma-ray energies are exhibited in Table 1. It should be mentioned that, the gamma emissions of ^{201}Tl (135 and 167 keV) occur in low abundance. Also, a schematic of the experimental setup is depicted in Figure 1, which demonstrates the utilized detection system including a point source of gamma-rays, the synthesized shield samples, a detector probe positioned behind the nanocomposite shields, along with a lead collimator. As shown in Figure 1 (right image), gamma ray energy peaks for a particular point source are shown using MCA.

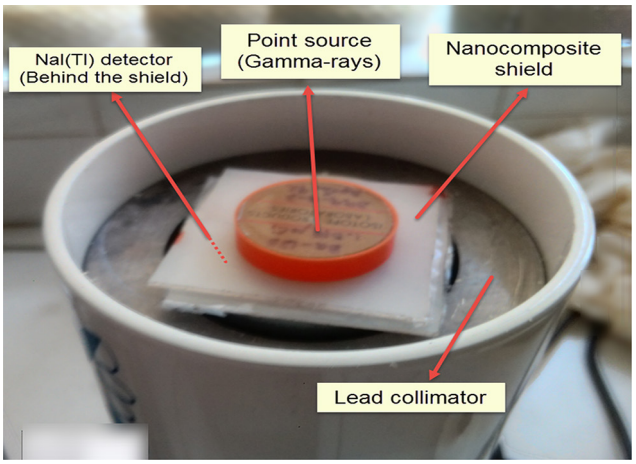
Simulation methodology: Geant4 toolkit

The Geant4 toolkit, a flexible Monte Carlo code implemented in the C++ programming language, has been developed to explore the behavior of electrons, neutrons, and photons when interacting with a specific medium. Geant4 utilizes its extensive cross-section database to effectively simulate particle interactions across a wide range of energy levels, spanning from 1 keV to 100 MeV. Also, it is organized into multiple segments, with the largest segment referred to as the universal size [35].

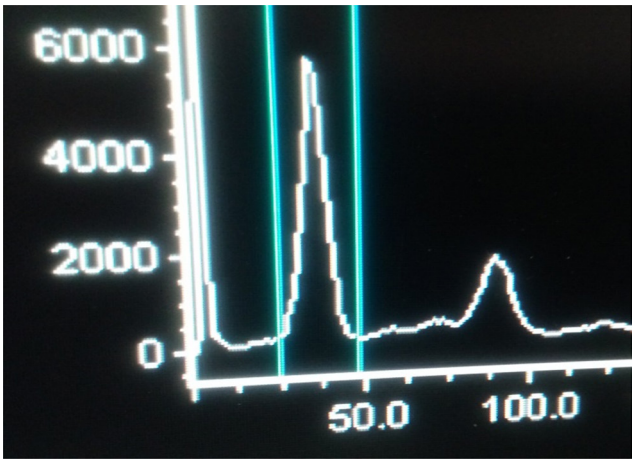
In this research, the Geant4 toolkit was used to simulate the radiation shielding characteristics of the WO_3/Polyethylene/Graphene oxide composite in different weight fractions against the gamma-rays of two sources of ^{201}Tl and ^{99m}Tc at three energies of 135, 140, and 167 keV. The calculation of photon attenuation involves simulating all pertinent physical processes and interactions that occur both before and after the insertion of the samples. The interaction of gamma-rays with matter is categorized to various mechanisms including the photoelectric effect,

Table 1. Gamma energy radioactive sources used for measuring the mass attenuation coefficients [33, 34].

Source	Half-life	Branching Ratio	Gamma Energy (keV)
^{201}Tl	73.1 hr	46.5% 27.4% 20.5% 2.5% 10%	70.8 68.9 80.3 135 167
^{99m}Tc	6 hr	88%	140



(a)



(b)

Figure 1. (a) The utilized detection system, and (b) peaks of gamma-rays obtained through the MCA.

Compton scattering, pair production, Rayleigh scattering, and also secondary electrons may produce Bremsstrahlung radiation, multiple scattering, and ionization [36, 37].

At the simulation phase using the Geant4 toolkit, to obtain the attenuation coefficients of the samples, varying thicknesses of the compounds were positioned between the point source and the detector utilizing a cylindrical NaI crystal. It should be noted that, a total of 1 million incident particles were consistently utilized. To validate the simulated data, a copper material (Z=29, and density of 8.96 g/cm^3) was used, along with a ^{137}Cs source emitting gamma-rays at 662 keV. The findings derived from the simulation analysis exhibited a 3% deviation from the expected values, signifying the satisfactory validation capability of the utilized code.

In order to ascertain the radiation shielding characteristics of a compound, it is imperative to consider the effect of heavy metal oxide concentrations. During the simulation phase, the weight percentages of the WO_3 particles are varied, encompassing values of 0, 1, 2, 3, 4, 5, 6, and 9.5 wt.%. The various concentrations of the inclusions allow for a comprehensive analysis of the compound's radiation shielding properties. For this purpose, a uniform effective medium in different thicknesses of 1, 2, 3 and 4 mm was considered with effective density which can be calculated as [38]:

$$\rho_c = \frac{1}{(W_f/\rho_f) + (W_m/\rho_m)} \quad (1)$$

In which ρ_c, ρ_f, and ρ_m are the density of the composite, filler, and matrix respectively; W_f and W_m are the weight fractions for the filler and matrix, respectively. Densities of WO_3, GO, HDPE, and LLDPE were considered as 7.16, 2.1, 0.95, and 0.92 g/cm^3, respectively.

A concise overview of the simulation process is provided herein. In order to provide a comprehensive description of the simulation geometry, the first step consisted of measuring the particle flux (I0) in the NaI (Tl) detector cell. This assessment was carried out in the absence of the composite shield to prevent any secondary radiations that could potentially impact the buildup factor (B). Thus, the setup of the geometry was configured as a narrow-beam within a specific energy window. Subsequently, the flux of particles (I) was evaluated in the detector cell with the composite shield in place. The composite surface was directly exposed to a point source that possessed a pre-established energy level, as specified in Table 1. The detector, situated behind the samples, captured the radiation emitted from this source. The linear attenuation coefficient (μ) can be calculated by plotting $\ln(I_0/I)$ against the shield thickness (x). The slope of this curve represents the value of the linear attenuation coefficient. The mass attenuation coefficient is then derived by dividing the linear attenuation coefficient by its density. By obtaining these coefficients, a deeper understanding of the shielding properties of the composites could be obtained [39]:

$$\mu = \frac{ln\left(\frac{I_0}{I}\right)}{x} \quad (2)$$

Moreover, the half-value layer (HVL) and tenth value layer (TVL) can be computed using the subsequent formulas [39]:

$$HVM = \frac{ln\,2}{\mu} \quad (3)$$

$$TVL = \frac{ln\,10}{\mu} \quad (4)$$

Preparation of the nanocomposite samples

Here, the details of preparation of the nanocomposite samples are explained. At first, high-density polyethylene (HDPE) was dissolved in an ortho-xylene solvent and subjected to heating at a temperature of 130°C for 15 min to achieve complete dissolution. Subsequently, WO_3 and GO powders, according to Table 2, were poured into separate containers including ortho-xylene and subjected to ultra-sonication for 10 minutes using an ultrasonic probe sonicator. It should be noted that in order to add LLDPE to the samples of I and J, it is necessary to consider that this polymer has a lower melting temperature compared to HDPE. Therefore, after complete dissolution of HDPE, the temperature of the solution is allowed to slightly decrease to 120°C, and then LLDPE is added to the solution and completely dissolved. Furthermore, polyethylene and nanoparticles are mixed together and the container containing the mixture is allowed to dry completely at room temperature for three days. Finally, the samples were optimized to be created in a steel mold with a thickness of 1.2 mm using the hot press, taking into account the HVL values during the experimental phase. Thus, the nanocomposite samples were placed in steel molds with dimensions of 8×8 cm^2

Table 2. Weight percentage and density for the twelve synthesized samples in this work.

Sample	WO_3 wt.%	GO wt.%	HDPE wt.%	LLDPE wt.%	Density (g/cm³)
A	1.00	0.25	98.75	0.00	0.96
B	3.00	0.25	96.75	0.00	0.98
C	5.00	0.25	94.75	0.00	0.99
D	6.00	0.25	93.75	0.00	1.00
E	1.00	0.50	98.50	0.00	0.96
F	2.00	0.50	97.50	0.00	0.97
G	3.00	0.50	96.50	0.00	0.98
H	4.00	0.50	95.50	0.00	0.99
I	1.00	0.00	89.00	10.00	0.96
J	1.00	0.00	79.00	20.00	0.95
K	9.50	1.00	89.50	0.00	1.04
L	0.00	0.00	100.00	0.00	0.95

and a thickness of 1.2 mm for hot pressing (ToyoSeiki model) at a temperature of 190°C. It is important to highlight that, in the hot pressing stage, the samples underwent an initial preheating process lasting 2 min, followed by a 5-min hot pressing phase at a pressure of 25 kg/cm^2, and concluded with a 3-min cold pressing phase at a pressure of 25 MPa.

RESULTS AND DISCUSSION

EDS analysis

The EDS or EDAX analysis as a non-destructive and highly accurate method plays an important role in evaluating the constituent materials of a compound. By bombarding the sample with a focused electron beam, the technique induces the emission of characteristic X-rays from the atoms present. These emitted X-rays are then detected and analyzed, allowing for the identification and quantification of the elements within the sample.

As shown in Figure 2, the EDS analysis of the sample A (containing of 1 wt.% WO_3, and 0.25 wt.% GO), was depicted, in which confirmed the presence of various atoms in the compound namely W, O, and C, by taking into account the several peaks for W (tungsten) including L_α, L_β, M_α.

SEM analysis

To investigate the dispersion state of the WO_3 nanoparticles, and GO nanoplates into the nanocomposite, and also to evaluate the effect of LLDPE on the quality of dispersion of the inclusions into the polymer matrix, SEM test was performed. Figure 3 illustrates the surface characteristics of the sample L (pure HDPE), revealing the presence of adjacent plate-like structures with diverse shapes and dimensions. These plates are separated by white streaks that act as boundaries. Additionally, the surface of polyethylene displays holes after being fabricated using a solution method. However, upon the incorporation of graphene oxide, these holes seem to vanish, resulting in a surface resembling that of pure polyethylene. This observation is evident in the sample E, which contains 1 wt.% WO_3 and 0.5 wt.% GO. This observation can be attributed to the presence of GO nanoplates in the material.

The bonding between graphene and polyethylene has the potential to enhance the amorphous region, thereby improving the dispersion of WO_3 nanoparticles [40]. However, the SEM images do not provide clear distinctions in the components and structures of polyethylene and graphene, making it difficult to differentiate between them. The presence of GO seems to have a significant impact on the surface morphology and properties of the polymer, indicating potential interactions at the nanoscale level. The unique characteristics of the polymer surface, influenced by the addition of GO, highlight the complex interactions between different materials at the nanoscale. The disappearance of holes on the polyethylene surface and the formation of distinct boundaries between plate-like structures suggest a transformation in the material's morphology due to the presence of GO. Further research is needed to fully understand the mechanisms behind these observations and to explore the potential applications of such modified polymer composites in various fields.

In general, the distribution of the WO_3 nano-fillers within the HDPE matrix indicates a fairly uniform dispersion of the particles. However, there are some agglomerations in the samples of C (containing 5 wt.% WO_3, and 0.25 wt.% GO), and K (containing 9.5 wt.%

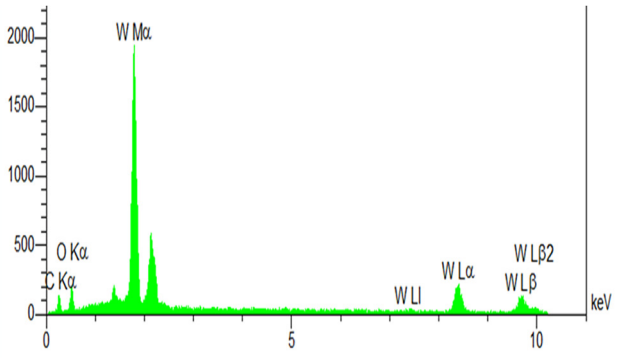


Figure 2. EDS analysis for sample "A" containing 1 wt.% WO_3, and 0.25 wt.% GO in the HDPE matrix, exhibiting the presence of tungsten atoms in the compound.

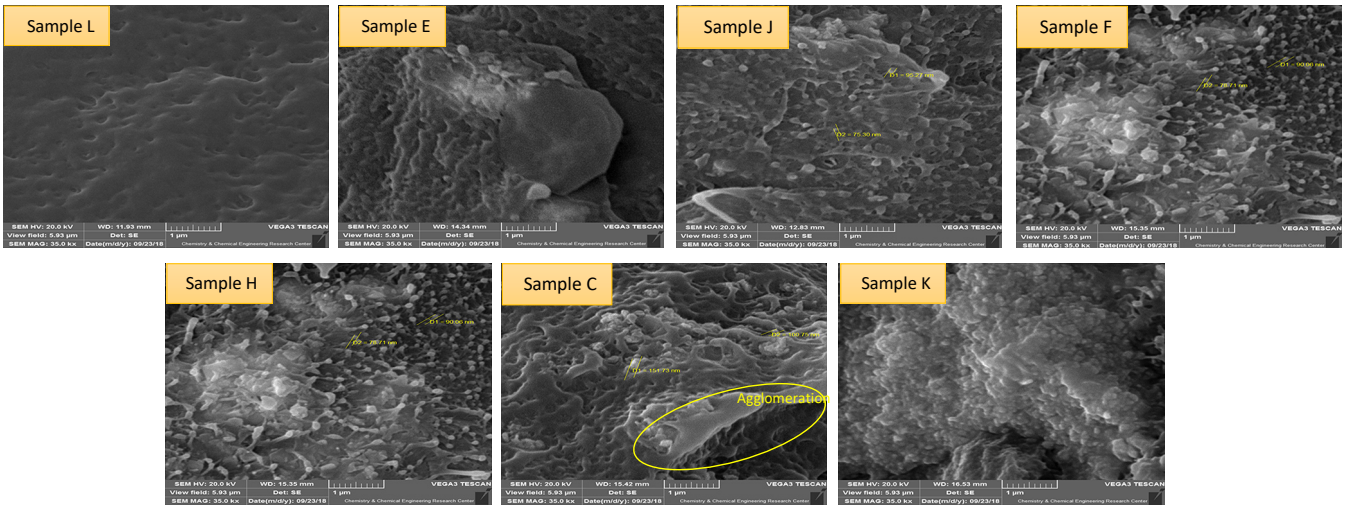


Figure 3. SEM images of various samples, exhibiting WO_3 nanoparticles at scale of 1 μm.

WO_3, and 1 wt.% GO). These agglomerations may have been formed due to the semi-crystalline nature of the HDPE matrix. Because the crystalline regions of the polymer often repel nanoparticles, so the nanoparticles are dispersed in the amorphous regions [22].

As can be seen from Figure 3, the sample J (containing 1 wt.% WO_3, and 20 wt.% LLDPE) exhibited a better dispersion state in comparison the sample E (containing 1 wt.% WO_3, and 0.5 wt.% GO). The analysis of Figure 3 reveals a remarkable expansion in the diameter of tungsten oxide nanoparticles when integrated into the polymer, now ranging from 70-150 nm. This is a substantial increase from the previous size range of 20 to 66 nanometers (based on the catalogue), attributed to the polymer matrix encapsulating the nanoparticle surfaces.

Simulation results

XCOM program

The XCOM program is applied for evaluating the X-rays and γ-rays attenuation coefficients and interaction cross sections [41]. As shown in Figure 4, the quantity of μ/ρ for WO_3-polyethylene composites containing 0.5 wt.% GO at different WO_3 wt.% and various energies were obtained using the XCOM program. The concentration level was evaluated up to 50 wt.%, however, there is no notable difference when incorporating 0.5 wt.% GO into the composite, due to low density and low concentration of grapheme oxide. The findings of the study indicate that as the energy of the incident photons increases, the material's ability to attenuate the photons decreases. However, there are certain cases where this trend is not observed, specifically at the absorption edges of the K, L, M, and N atomic layers.

At these edges, the attenuation coefficient unexpectedly increases. This phenomenon can be attributed to the photoelectric absorption cross section, which experiences a surge at the absorption edges. Consequently, photons with energies corresponding to these edges are fully absorbed by the material, resulting in the removal of photoelectrons from the atom. Also, it should be mentioned that the absence of any absorption edge in pure polyethylene is evident in Figure 4. Nevertheless, the incorporation of the WO_3 particles into the polymer matrix causes the appearance of absorption edges.

In this regard, Table 3 provides a comprehensive overview of the various absorption edges associated with tungsten at different energy levels.

It should be noted that according to the test STAGE and especially for higher loadings, the simulation results may be different from the results obtained from the experimental tests.

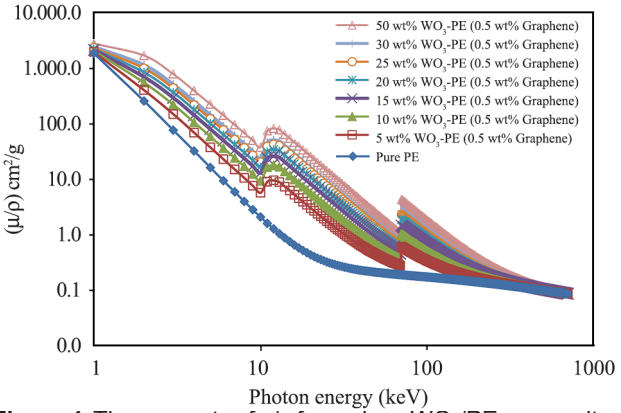


Figure 4. The amounts of μ/ρ for various WO_3/PE composites containing 0.5 wt.% graphene at different energies using the XCOM program.

Table 3. Absorption edges of the tungsten at various energies [42].

Edge	Energy (keV)
K	69.525
L1	12.0998
L2	11.5440
L3	10.2068
M1	2.8196
M2	2.5749
M3	2.2810
M4	1.8716
M5	1.8092

Comparison of Experiment, Geant4, and XCOM results

In this section, as can be seen from Table 4, and Figures 5-8, the values of μ, and μ/ρ, HVL and TVL quantities related to the various samples (based on Table 2) at different concentrations were obtained at three energies of 135, 140, and 167 keV using experiment (Exp), Geant4, and XCOM. It should be mentioned that during the measurement using a NaI (Tl) scintillation detector, count vs. channel number was depicted for various thicknesses of the samples against the gamma-rays of the ^{201}Tl (two main peaks of 135, and 167 keV), and ^{99}mTc sources (140 keV). The linear attenuation coefficient of the nanocomposite shield was determined via the summation of the area under the curve (AUC) at specified energies. The AUC at various energies was decreased as the nanocomposite thickness increased. It is important to note that four nanocomposite layers, each with a thickness of 1.2 mm, were placed adjacent to each other during the measurement, varying from one layer to four layers.

Table 4 clearly shows that the measured values of μ/ρ at various energy levels are notably greater than those predicted by XCOM and Geant4 simulations. This discrepancy can be attributed to the exceptional surface-to-volume ratio of WO_3 nanoparticles, which enhances their effectiveness in radiation shielding applications.

As depicted in Figures 5 and 6, for the samples, the amounts of μ and μ/ρ increased with increasing the WO_3 wt.%. This could be attributed to the increased density of the composite, regarding the fact that the probability of the photoelectric effect increases for high Z materials at low energy photons as $Z^n/E^{3.5}$, in which Z is atomic number of the absorber material, E is the photon or X-rays energy, and n is a variable exponent between 4 and 5 [43].

In the experimental phase, as depicted in Figure 5 at 140 keV, results indicate that the addition of LLDPE to the HDPE polymer matrix for the ^{99}mTc source at 20 wt.% for sample J leads to a significant increase in the linear attenuation coefficient of this material by 18% compared to the material without LLDPE, namely sample A (containing 1 wt.% WO_3, and 0.25 wt.% GO)

In explaining this concept, it can be argued that the presence of LLDPE may have caused a decrease in the crystalline area and consequently, an increase in the amorphous region within the nanocomposite. This, in turn, allows for a more homogeneous dispersion of tungsten oxide nanoparticles in the polymer matrix, which can be observed in the SEM images for sample J in Figure 3.

In the experimental phase, at 140 and 167 keV, the fact that the μ and μ/ρ for the sample K (containing of 9.5 wt.% WO_3) with respect to sample C (containing of 5 wt.% WO_3) are significantly lower can be attributed

Table 4. Comparison of mass attenuation coefficients for various samples, using Geant4, XCOM, and experiment.

Sample	(μ/ρ)-cm²/g								
	135 keV			140 keV			167 keV		
	Geant4	XCOM	Exp	Geant4	XCOM	Exp	Geant4	XCOM	Exp
L	0.1558	0.1589	0.1605±0.0144	0.1548	0.1579	0.1595±0.0144	0.1462	0.1491	0.1506±0.0136
A	0.2408	0.1735	0.2497±0.0225	0.2309	0.1704	0.2186±0.0197	0.1959	0.1569	0.1900±0.0171
E	0.2407	0.1737	0.2433±0.0219	0.2314	0.1705	0.2547±0.0229	0.1965	0.1757	0.2910±0.0262
I	0.2395	0.1733	0.3814±0.0343	0.1754	0.1702	0.2173±0.0196	0.1949	0.1569	0.4313±0.0388
J	0.2405	0.1733	0.3343±0.0301	0.1768	0.1702	0.2628±0.0237	0.1969	0.1569	0.4857±0.0437
F	0.2053	0.1888	0.3307±0.0298	0.2002	0.1842	0.2701±0.0243	0.1790	0.1654	0.3185±0.0287
B	0.3216	0.2036	0.3491±0.0314	0.3101	0.1977	0.2822±0.0254	0.2638	0.1737	0.3001±0.0270
G	0.2643	0.2038	0.5360±0.0482	0.2240	0.1978	0.3161±0.0284	0.2150	0.1738	0.4760±0.0428
H	0.2766	0.2189	0.5676±0.0511	0.2512	0.3115	0.6837±0.0615	0.2262	0.1822	0.4879±0.0439
D	0.3025	0.2338	0.5065±0.0456	0.3070	0.2250	0.5457±0.0491	0.2458	0.1905	0.4756±0.0428
K	0.3374	0.2489	0.7075±0.0637	0.3250	0.2386	0.4739±0.0427	0.2746	0.1989	0.5049±0.0454
C	0.2915	0.3018	0.6450±0.0581	0.2791	0.2865	0.6367±0.0573	0.2373	0.2283	0.5745±0.0517

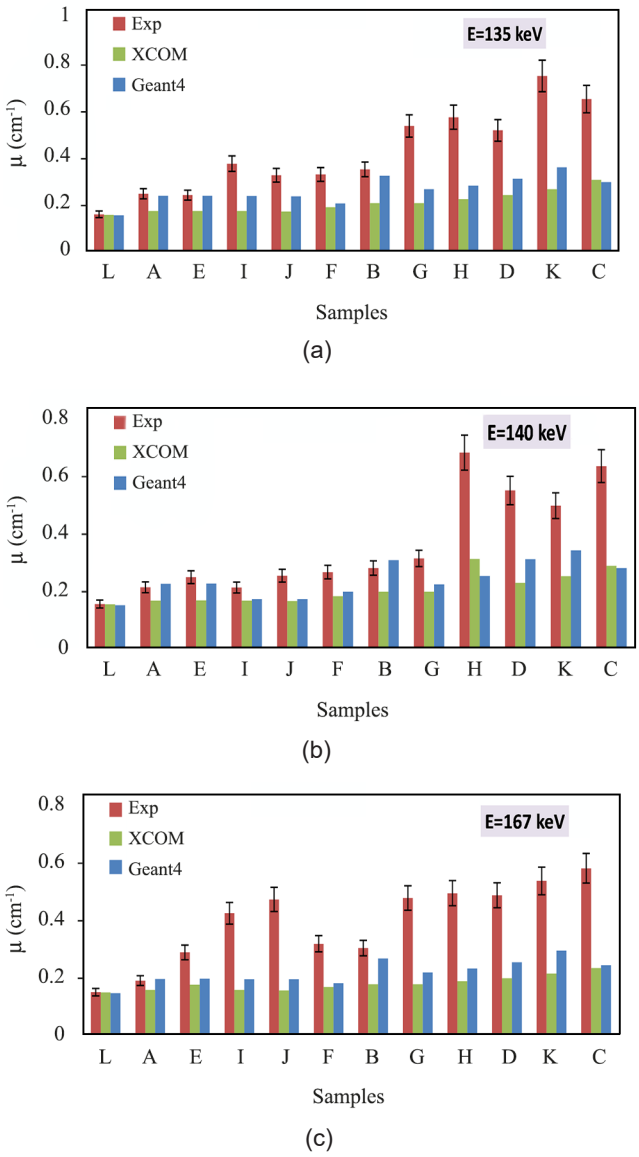


Figure 5. Attenuation coefficient (μ) of various samples at three energies of (a) 135, (b) 140, and (c) 167 keV using experiment (Exp), XCOM, and Geant4.

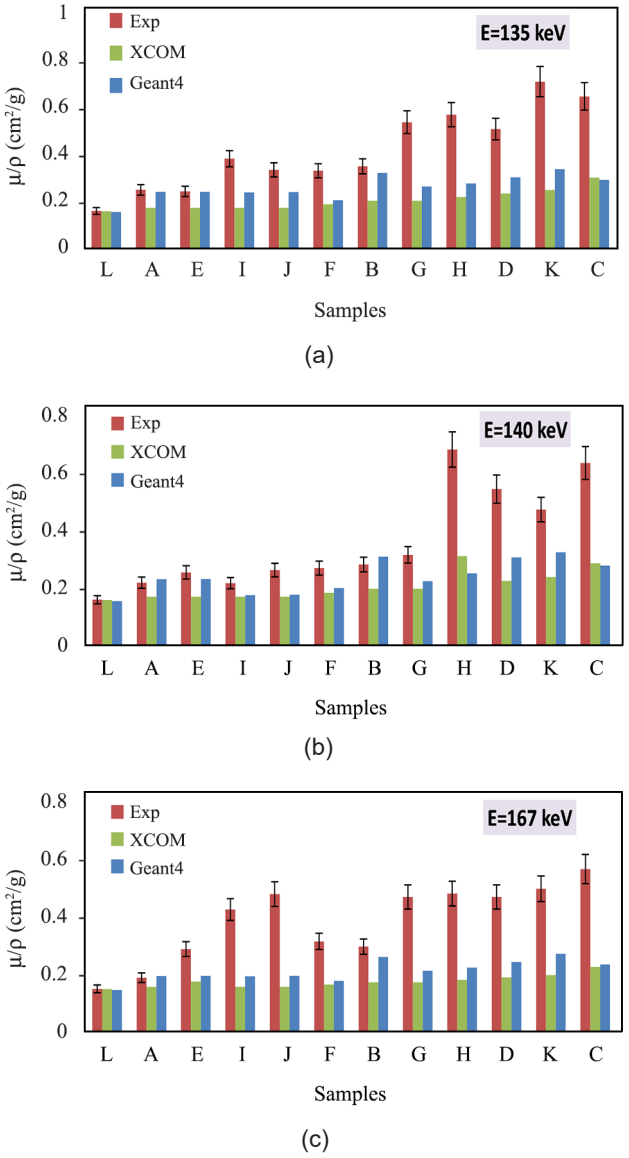


Figure 6. Mass attenuation coefficient (μ/ρ) of various samples at three energies of (a) 135, (b) 140, and (c) 167 keV using experiment, XCOM, and Geant4.

to the observation, as evident from the SEM images, that agglomeration occurs at higher levels of the WO_3 concentrations, specifically at 9.5 wt.% for sample K, in which the WO_3 nanoparticles are not uniformly dispersed. Consequently, the value of the attenuation coefficients for sample K decreases in comparison with sample C.

It is evident from Figures 7 and 8 that by adding the concentration of WO_3 particles into the polymer matrix, the HVL and TVL quantities decrease significantly. This reduction is reasonably consistent with the results obtained through the Geant4, XCOM, and experimental data, for various samples.

The experimental results exhibited a significant increase to μ/ρ in comparison with the Geant4, and XCOM simulations at various energies. This increase may be pertinent to this fact that the nano-fillers exhibit excellent surface-to-volume ratio and higher photon absorption cross section against the gamma-rays and X-rays than micro-fillers based on the other studies [1, 44-48].

In Table 5, a comparison of μ/ρ, HVL, and TVL is exhibited for samples of H, C, D, and K with several reference materials including lead, glass-lead, concrete-barite, concrete-ordinary, and polyethylene. As can be easily seen from Table 5, radiation shielding effectiveness of sample K (containing of 9.5 wt.% WO_3) is better than that of concrete-barite, and

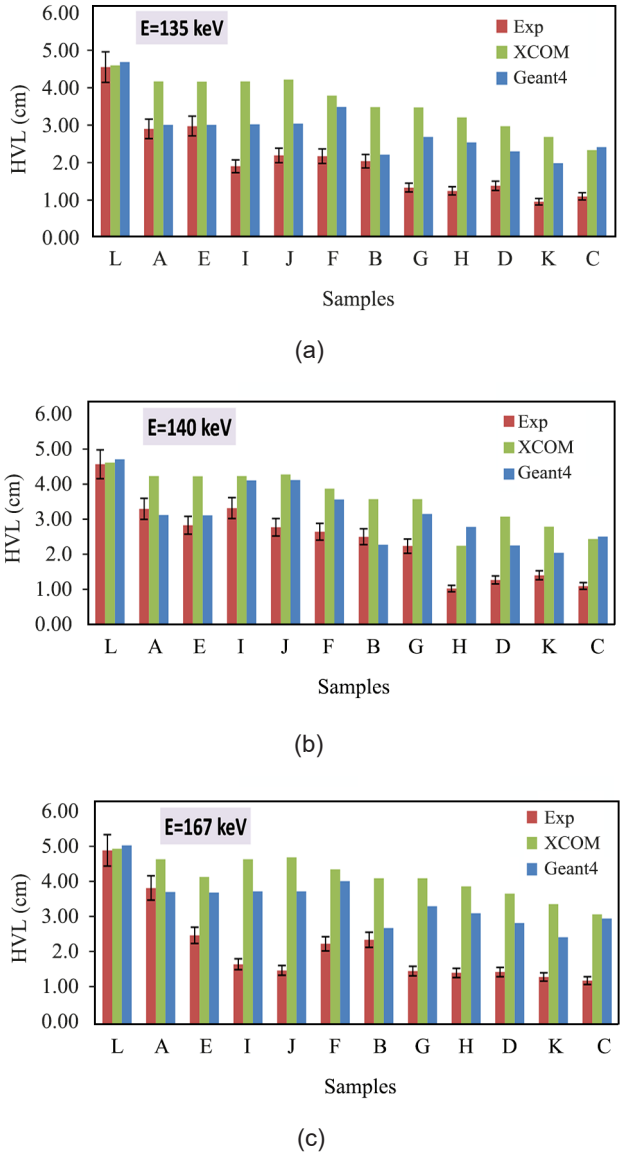


Figure 7. Half-value layer (HVL) of various samples at three energies of (a) 135, (b) 140, and (c) 167 keV using experiment, XCOM, and Geant4.

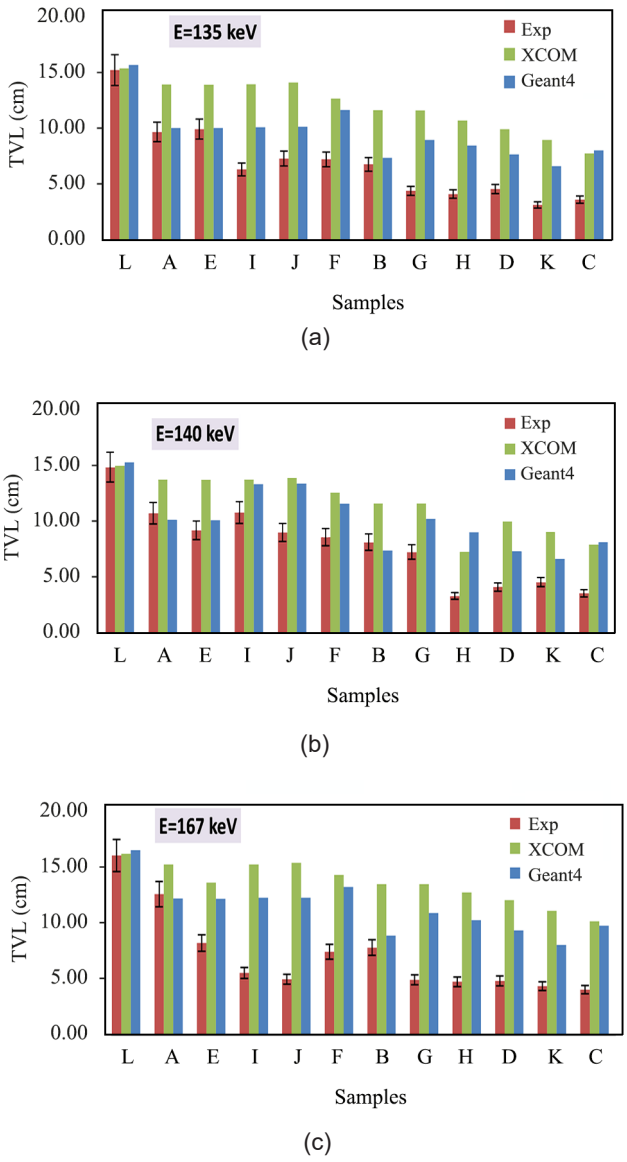


Figure 8. Tenth-value layer (TVL) of various samples at three energies of (a) 135, (b) 140, and (c) 167 keV using experiment, XCOM, and Geant4.

concrete-ordinary. However, lead and glass-lead have higher mass attenuation coefficients than polymer-heavy metal oxide nanocomposite samples at low energies. Nevertheless, challenges arise due to the toxicity of lead and its secondary radiations, leading to a balance or compromise between lower toxicity and higher HVL and TVL values for lead-free polymer-heavy metal oxide nanocomposites.

To estimate the uncertainty at the experimental phase, two kinds of uncertainties namely type A (u_A) related to the random statistical error (5%), and type B (u_B) pertinent to the systematic error and accuracy due to calibration of the NaI (Tl) scintillator (±7.5%) were considered. Thus, the combined uncertainty (u_C) can be derived as [49]:

$$u_C = \sqrt{(u_A)^2 + (u_B)^2} \quad (5)$$

It should be noted that despite the potential environmental and safety concerns posed by heavy metal oxide compounds [50], such as WO_3, they can still be recycled using photocatalyst materials [51].

CONCLUSION

In recent years, there has been a significant trend

Table 5. Comparison of mass attenuation coefficients of prepared samples in this work (experimental values) and several standard materials using the XCOM program [42].

Sample	ρ (g/cm³)	135 keV			140 keV			167 keV		
		(μ/ρ)-cm²/g	HVL (cm)	TVL (cm)	(μ/ρ)-cm²/g	HVL (cm)	TVL (cm)	(μ/ρ)-cm²/g	HVL (cm)	TVL (cm)
Lead	11.36	2.634	0.023	0.077	2.383	0.026	0.085	1.563	0.039	0.130
Glass, lead	6.22	2.017	0.055	0.184	1.828	0.061	0.203	1.324	0.084	0.280
Concrete, Barite	3.35	0.5616	0.368	1.224	0.5140	0.403	1.337	0.3891	0.532	1.766
Concrete, Ordinary	2.30	0.1500	2.009	6.674	0.1476	2.042	6.783	0.1374	2.193	7.286
Polyethylene	0.93	0.1580	4.717	15.670	0.1564	4.765	15.831	0.1503	4.959	16.473
Sample H (This work)	0.99	0.5676	1.234	4.098	0.6837	1.024	3.402	0.4879	1.435	4.767
Sample C (This work)	0.99	0.645	1.086	3.606	0.6367	1.100	3.653	0.5745	1.219	4.048
Sample D (This work)	1.00	0.5065	1.369	4.546	0.5457	1.270	4.220	0.4756	1.457	4.841
Sample K (This work)	1.04	0.7075	0.942	3.129	0.4739	1.406	4.672	0.5049	1.320	4.385

towards the use of lead-free radiation shielding materials as a solution to the challenges posed by lead. Despite its effectiveness in radiation protection and widespread availability, lead has several drawbacks, including its high toxicity, low mechanical strength, heavy weight, and the potential for dangerous hospital pathogens to survive on lead aprons. One possible solution is to utilize appropriate polymers as a matrix and incorporate heavy metal oxide particles as fillers. This study investigates the radiation shielding properties of high-density polyethylene (HDPE) nanocomposites infused with tungsten oxide (WO_3) nanoparticles and further reinforced with graphene oxide (GO) and linear low-density polyethylene (LLDPE). The study evaluates key parameters such as the linear attenuation coefficient (μ), mass attenuation coefficient (μ/ρ), half-value layer (HVL), and tenth-value layer (TVL) for photon energies using Geant4 simulations, XCOM database, and experimental methods. The study uses HDPE as the polymer matrix with varying concentrations of WO_3 nanoparticles (0 to 9.5 wt.%), GO (0 to 1 wt.%), and LLDPE (10 and 20 wt.%). The nanocomposites were tested using a NaI (Tl) scintillation detector with photon energies of 135, 140, and 167 keV from Thallium-201 and Technetium-99m sources. Geant4 simulations and XCOM database calculations were validated against experimental results.

At the experimental phase, based on the SEM images, the addition of GO and LLDPE exhibited a more uniform dispersion of WO_3 nanoparticles, enhancing the attenuation coefficients. The linear and mass attenuation coefficients increased at higher WO_3 concentrations. The presence of GO at low levels (less than 1 wt.%) and LLDPE (at 20 wt.%) improved the dispersion of WO_3 nanoparticles. For instance, incorporating 20% LLDPE into the HDPE polymer matrix for the ^{99}mTc resulted in an 18% rise in μ compared to pure HDPE. Experimental results showed good agreement with Geant4 and XCOM simulations, particularly noting higher surface-to-volume ratios for nano-fillers that significantly improved attenuation. Also, sample K, which contains 9.5 wt.% WO_3, demonstrated superior radiation shielding effectiveness compared to several reference materials including concrete-barite and concrete-ordinary at energies of 135, 140, and 167 keV. HDPE/WO_3 nanocomposites, particularly when reinforced with GO and LLDPE, demonstrate effective radiation shielding properties for low-energy gamma and X-rays, making them suitable substitutes for lead-based shields in diagnostic applications.

ACKNOWLEDGEMENTS

We appreciate those who supported us in carrying out this project, especially Dr. M. Mirzaei, and Dr. A. Moslehi from the NSTRI, and we are always indebted to them for the success of this study.

CONFLICT OF INTEREST

The authors declare that they have no known competing financial interests or personal relationships that could have appeared to influence the work reported in this paper.

REFERENCES

1. Hosseini MA, Malekie S, Kazemi F (2022) Experimental evaluation of gamma radiation

shielding characteristics of polyvinyl alcohol/ tungsten oxide composite: A comparison study of micro and nano sizes of the fillers. Nucl Instrum Meth A 1026: 166214
2. Issa SA, Alrowaily AW, Abulyazied DE, Ali ES, Zakaly HM (2023) Effects of WO_3 reinforcement on the properties of poly (lactic acid) composites for radiation shielding. Radiat Phys Chem 212: 111121
3. Atta MM, Abou-Laila MT, Abdelwahed MH, Dwidar SA, Desouky O (2023) Structural, mechanical, and thermal features of PVA/starch/ graphene oxide nanocomposite enriched with WO_3 as gamma–ray radiation shielding materials for medical applications. Polym Eng Sci 63: 3843-3854
4. Mehrara R, Malekie S, Kotahi SM, Kashian S (2021) Introducing a novel low energy gamma ray shield utilizing Polycarbonate Bismuth Oxide composite. Sci Rep 11: 10614
5. Mourad M, Abdou Y, Berber MR, Elhussiny F (2021) Using nano tungsten oxide polymer composite as a gamma radiation shielding. Delta J Sci, 43: 126-132
6. Abdolahzadeh T, Morshedian J, Ahmadi S (2022) Preparation and characterization of nano WO_3/Bi_2O_3/GO and $BaSO_4$/GO dispersed HDPE composites for X-ray shielding application, Polyolefins J 9: 73-83
7. Olivieri F, Avolio R, Gentile G, Mazzone A, Rizzi R, Nacucchi M, Castaldo R, Errico ME, Giannini C, Ambrosio L, Lavorgna M. (2024) High filler content acrylonitrile-butadiene-styrene composites containing tungsten and bismuth oxides for effective lead-free x-ray radiation shielding. Polymer Compos, 45: 2101-2113
8. Malekie S, Kashian S, Akhavan A, Kheradmand-Saadi M (2023) Preliminary study of a novel radiation shield for jaw in dental radiography using the high-density polyethylene/bismuth oxide nanocomposite. Radiat Phys Chem 205: 110743
9. Kilicoglu O, More CV, Kara U, Davraz M (2023) Investigation of the effect of cement type on nuclear shield performance of heavy concrete. Radiat Phys Chem 209: 110954
10. Vignesh S, Winowlin Jappes JT, Nagaveena S, Krishna Sharma R, Adam Khan M, More CV, Rajini N, Varol T (2022) Development of lightweight polymer laminates for radiation shielding and electronics applications. Int J Polym Sci 2022: 5252528
11. Ali ES, Issa SA, Zakaly HM, El-Shamy NT, Saudi HA, Abulyazied DE (2024) Exploration of optical and gamma radiation shielding characteristics of zinc oxide nanoparticles doped functionalized multi-walled carbon nanotubes nanohybrids based polyaniline ternary nanocomposites. Diam Relat Mater 143: 110882
12. Başgöz Ö, Güler SH, Güler Ö, Canbay CA, Zakaly HM, Issa SA, ALMisned G, Tekin HO (2022) Synergistic effect of boron nitride and graphene nanosheets on behavioural attitudes of polyester matrix: Synthesis, experimental and Monte Carlo simulation studies. Diam Relat Mater 126: 109095
13. Issa SA, Zakaly HM, Tekin HO, Saudi HA, Badawi A, Pyshkina M, Susoy G, Elazaka AI, Ene A (2021) Exploring the FTIR, optical and nuclear radiation shielding properties of samarium-borate glass: a characterization through experimental and simulation methods. Nanomaterials 11: 1713
14. Khalil HF, Malidarreh RB, Alabsy MT, Hassan AM, El-Khatib AM, Issa SA, Zakaly HM (2024) Structural, morphological, and γ-ray attenuation properties of m-type hexaferrite BaFe12O19 doped with V2O5, Ce_2O_3 and Bi_2O_3 for radiation shielding applications. Ceram Int 50: 33771-33780
15. Zakaly HM, Issa SA, Saudi HA, Alharshan GA, Uosif MA, Henaish AM (2022) Structure, Mössbauer, electrical, and γ-ray attenuation-properties of magnesium zinc ferrite synthesized co-precipitation method. Sci Rep 12: 15495
16. Almuqrin AH, Rashad M, More CV (2024) Sayyed MI, Elsafi M. An experimental and theoretical study to evaluate Al_2O_3–PbO–B_2O_3-SiO_2-BaO radiation shielding properties. Radiat Phys Chem 222: 111824
17. Sayyed MI, Kaky KM, Mhareb MH, Imheidat MA, Es-soufi H, Kadhim AJ, Baki SO (2024) The influence of MgO on the physical, structural, mechanical, optical, and radiation absorption properties of the boro-germanate glass system. Ceram Int 50: 33618-33629
18. Gaikwad KB, Gattu KP, More CV, Pawar PP (2024) Physical, structural and nuclear radiation shielding behavior of Ni-Cu-Zn Fe_2O_4 ferrite

nanoparticles. Appl Radiat Isot 207: 111244
19. More CV, Akman F, Dilsiz K, Ogul H, Pawar PP (2023) Estimation of neutron and gamma-ray attenuation characteristics of some ferrites: Geant4, FLUKA and WinXCom studies. Appl Radiat Isot 197: 110803
20. Mehnati P, Malekzadeh R, Sooteh MY (2020) Application of personal non-lead nano-composite shields for radiation protection in diagnostic radiology: a systematic review and meta-analysis. Nanomed J 7170-182
21. Paul S, Chaturvedi K, Suresh S, Mili M, Bajpai H, Parmar V, Bhopche R, Khan MA, Srivastava AK, Verma S (2024) A review on radiation shielding materials based on low-strength chemical wastes and nanomaterials. Adv Radiat Shield Mater 2024: 227-250
22. Safdari SM, Malekie S, Kashian S, Akbari M (2022) Introducing a novel beta-ray sensor based on polycarbonate/bismuth oxide nanocomposite. Sci Rep 12: 2496
23. Patil AP, Gaikwad MA, Nadargi JD, Shaikh H, Alam MA, Tamboli MS, Kim JH, Mulla IS, Suryavanshi SS (2024) Reduced graphene oxide/tungsten oxide (rGO/WO_3): A versatile nanocomposite for enhanced detection of acetone. J Mater Sci: Mater Electron 35: 264
24. Rotkovich AA, Tishkevich DI, Razanau IU, Vershinina TN, Bondaruk AA, German SA, Zubar TI, Sayyed MI, Dong M, Yao Y, Mahmoud KA (2024) Development and study of lightweight recycled composite materials based on linear low-density polyethylene and W for radiation application. J Mater Res Technol 30: 1310-1318
25. Tekin HO (2016) MCNP-X Monte Carlo Code Application for Mass Attenuation Coefficients of Concrete at Different Energies by Modeling 3× 3 Inch NaI (Tl) Detector and Comparison with XCOM and Monte Carlo Data. Sci Technol Nucl Ins 2016: 6547318
26. Malekie S, Hajiloo N (2017) Comparative study of micro and nano size WO_3/E44 epoxy composite as gamma radiation shielding using MCNP and experiment. Chin Phys Lett 34: 108102
27. Kazemi F, Malekie S (2019) A Monte Carlo study on the shielding properties of a novel polyvinyl alcohol (PVA)/WO_3 composite, against gamma rays, using the MCNPX code. J Biomed Phys Eng 9: 465-472
28. Shooli H, Malekie S, Hosseini MA (2020) Preliminary studies on nanocomposites containing PA6/WO_3 as X-ray and gamma-ray shields using the Monte Carlo method, 14th International Seminar on Polymer Science and Technology (ISPST 2020), Tarbiat Modares University, Tehran, Iran
29. Keshavarzi M, Malekie S, Hosseini MA (2020) An overview of the radiation-protective properties of nanocomposites containing iron oxide and high density polyethylene in the presence of X- and gamma-rays, 14th International Seminar on Polymer Science and Technology (ISPST 2020), Tarbiat Modares University, Tehran, Iran
30. Adeli R, Shirmardi SP, Ahmadi SJ (2016) Neutron irradiation tests on B_4C/epoxy composite for neutron shielding application and the parameters assay. Radiat Phys Chem 127: 140-146
31. Adeli R, Shirmardi SP, Bagheri R (2017) Theory and simulation investigation of low-energy neutron shielding for different boron compounds. J Test Eval 45: 1570-1576
32. Tan JZ, Ortega M, Miller SA, Hullfish CW, Kim H, Kim S, Hu W, Hu JZ, Lercher JA, Koel BE, Sarazen ML (2024) catalytic Consequences of hierarchical pore architectures within MFI and FAU zeolites for polyethylene conversion. ACS Catal 14: 7536-7552
33. Helene OA, Vanin VR, Helmer RG, Schönfeld E, Dersch R, Baglin CM, Browne E, Castro RM, Pascholati PR (2007) Update of X-ray and gamma-ray decay data standards for detector calibration and other applications. IAEA, Vienna, 210
34. Grupen C (2010) A Table of Frequently Used Radioisotopes, Springer, pp. 323
35. Alabsy MT, Alzahrani JS, Sayyed MI, Abbas MI, Tishkevich DI, El-Khatib AM, Elsafi M (2021) Gamma-ray attenuation and exposure buildup factor of novel polymers in shielding using Geant4 simulation. Materials 14: 5051
36. Aghdam SR, Aghamiri SM, Malekie S, Mosayebi A (2023) Performance characteristics of a parallel plate dosimeter based on PVA/MWCNT-OH nanocomposite for photon beam radiation. Measurement 207: 112419
37. Aghdam SR, Aghamiri SM, Malekie S, Mosayebi A (2023) Evaluating the linearity response for a PVA/MWCNT-OH nanocomposite dosimeter in photon beam of linear accelerator. Radiat Phys

Chem 210 (2023) 111044
38. Rahman A, Singh A, Karumuri S, Harimkar SP, Kalkan KA, Singh RP (2015) Graphene reinforced silicon carbide nanocomposites: processing and properties. In: Composite, hybrid, and multifunctional materials. Vol. 4, Springer, pp. 165-176
39. Cember H, Johnson TE (2009) Introduction to health physics, 4th Ed, McGraw-Hill, New York
40. Papageorgiou DG, Kinloch IA, Young RJ (2017) Mechanical properties of graphene and graphene-based nanocomposites. Progr Mater Sci 90: 75-127
41. Berger MJ, Hubbell J (1987) XCOM: Photon cross sections on a personal computer, National Bureau of Standards, Washington, DC (USA)
42. Boone JM, Chavez AE (1996) Comparison of x-ray cross sections for diagnostic and therapeutic medical physics. Medical Phys 23: 1997-2005
43. Knoll GF (2010) Radiation Detection and Measurement, 4th Ed., John Wiley & Sons, Inc, University of Michigan, USA
44. Hołyńska B (1969) Grain size effect in low energy gamma and X-ray scattering. Spectrochim Acta B Atom Spectrosc 24: 85-93
45. Asgari M, Afarideh H, Ghafoorifard H, Amirabadi EA. Comparison of nano/micro lead, bismuth and tungsten on the gamma shielding properties of the flexible composites against photon in wide energy range (40 keV–662 keV). Nucl Eng Technol 53: 4142-4149
46. Azman NN, Siddiqui SA, Low IM (2013) Characterisation of micro-sized and nano-sized tungsten oxide-epoxy composites for radiation shielding of diagnostic X-rays. Mater Sci Eng C 33: 4952-4957
47. Adliene D, Griskonis E, Vaiciunaite N, Plaipaite-Nalivaiko R (2015) Evaluation of new transparent tungsten containing nanocomposites for radiation protection screens. Radiat Protect Dos 165: 406-409
48. El-Khatib AM, Abbas MI, Elzaher MA, Badawi MS, Alabsy MT, Alharshan GA, Aloraini DA (2019) Gamma attenuation coefficients of nano cadmium oxide/high density polyethylene composites. Sci Rep 9: 16012
49. International Standards Organization, Guide to the Expression of Uncertainty in Measurement, ISO, Geneva (1993)
50. Zhang Q, Wu Y, Yuan H (2020) Recycling strategies of spent V_2O_5-WO_3/TiO_2 catalyst: A review. Resour Conserv Recycl 161: 104983
51. Khan MY, Ahmad M, Sadaf S, Iqbal S, Nawaz F, Iqbal J (2019) Visible light active indigo dye/graphene/WO_3 nanocomposites with excellent photocatalytic activity. J Mater Res Technol 8: 3261-3269